processes

MDPI

Article

Moisture Transport Coefficients Determination on a Model Pharmaceutical Tablet

Komlan Koumbogle, François Gitzhofer * and Nicolas Abatzoglou *

Department of Chemical and Biotechnological Engineering, Université de Sherbrooke, 2500 Boulevard de l'Université, Sherbrooke, QC J1K 2R1, Canada; komlan.koumbogle@usherbrooke.ca

* Correspondence: francois.gitzhofer@usherbrooke.ca (F.G.); nicolas.abatzoglou@usherbrooke.ca (N.A.)

Abstract: In this work, a novel methodology to determine moisture transport coefficients for MMC PH101 tablets is presented. Absolute permeability, moisture diffusion, moisture transfer, and water vapor permeability coefficients were estimated on compressed powder tablets produced with different compression pressures (20 MPa to 200 MPa with an interval of 20 MPa). The ASTM D6539 standard test was used to measure the absolute permeability. The moisture transfer coefficient was determined from measured absolute permeability. The moisture diffusion coefficient was obtained with the tablet average pore radius, which was determined with the water droplet penetration method. Descriptive and phenomenological models derived from the measurements were confronted with existing and adopted models, and a good agreement was found. The obtained models are of the function of the microstructural properties of the tablet (average pore radius and average porosity). The tablet average porosity was found to be the principal parameter that governs the behavior of the moisture transport coefficients. The findings of this study might be applicable to obtain a series of input parameters for modelling software, such as COMSOL Multiphysics®, to infer delamination, sticking, and failure propensity from the effect of moisture.

Keywords: pharmaceutical tablets; moisture; water vapor; water vapor permeability (WVP); moisture diffusion coefficient (MDC); moisture transfer coefficient (MTC); contact angle; microcrystalline cellulose PH101; Carman–Kozeny

Citation: Koumbogle, K.; Gitzhofer, F.; Abatzoglou, N. Moisture Transport Coefficients Determination on a Model Pharmaceutical Tablet. *Processes* **2022**, *10*, 254. https://doi.org/10.3390/pr10020254

Academic Editors: Ioannis Nikolakakis and Nizar Al-Zoubi

Received: 31 October 2021
Accepted: 20 January 2022
Published: 27 January 2022

1. Introduction

Pharmaceutical tablets are produced by the direct compression of powder during the tableting process. The compressed powder is often a blend of pharmaceutical powders (excipients and active ingredients) with different chemical natures [1]. Some of the powders in the blend are highly hygroscopic [2–5], which means that they are more likely to adsorb moisture from the ambient environment. Newman et al. [6] outlined a hygroscopicity classification scheme based on the rate and amount of water uptake from the atmosphere with changes in the air humidity. A non-hygroscopic powder shows almost no change in moisture content with exposure to air below 90% relative humidity, while the moisture content of a very hygroscopic powder would increase even in air with a relative humidity as low as 40–50%. The water content of microcrystalline cellulose (MCC), hydroxypropyl methylcellulose (HPMC), carboxymethyl cellulose (CMC), polyvinylpyrrolidone (PVP), corn starch, and potato starch, for instance, was found to increase at different rates with the increase of ambient relative humidity [7]. Newman et al. [6] indicated a possible range in relative humidity from 25 to 75% at a temperature of 25 °C for normal pharmaceutical handling conditions. Zografi et al. [8] reported a moisture content of 5–6% for microcrystalline cellulose (MCC) during routine handling under ambient conditions of 40–50% relative humidity. Partheniadis et al., through monitoring the weight and dimensional expansion under dynamic vapor sorption, reported that the weight and dimension of pyridostigmine bromide tablets increases with the ambient relative humidity due to the increase of the

tablet moisture [9]. Shi et al. [10] proposed a typical moisture content of 3–5% for MCC under ambient conditions and showed that there were major property changes within this range. Sun et al. [1] also found variations in MCC properties within the small 3–5% moisture range but concluded that this range was still ideal, as more significant property changes were observed at higher moisture levels. These previous studies show how the moisture content of pharmaceutical powder can change during handling and manufacturing.

Water in powders can be in different physical states [6]: (1) adsorbed monolayer or multilayers on the surfaces of the particle, (2) condensed water on the particle surface, (3) physically absorbed water within the particle, or (4) chemisorbed water. The state and distribution of the water depends on the powder and the amount of water taken up through exposure to humid air and affects many properties of the powder. F. Khan et al. [11] found that, above a water content of 3 wt.%, water forms as a film on the surfaces of the particles. It acts as a lubricant, plasticizing asperities and facilitating the rearrangement of the particles during densification and compaction. Hence, the plastic deformation during the compression and the elastic recovery after the compression decrease. Below 3 wt.%, the plastic deformation increases the contact area and the amount of hydrogen bonding between the hydroxyl groups on the surface of the particles. The tensile strength and Young modulus of the material both initially increase with the water content. However, above 3wt.%, the moisture begins to disrupt these bonds, and this could account for the subsequent decrease in the values of tensile strength and Young modulus. Crouter et al. [7] found that the flowability of MCC, CMC, PVP, and potato starch decreased after a critical moisture content by forming stronger interparticle liquid bridges and increasing the flowability of corn starch. The moisture decreased flowability by forming stronger interparticle liquid bridges and increased flowability by acting as a lubricant. Furthermore, the dynamic density of some particles, such as PVP and starch, decreased with increasing moisture as the particles swelled with water. S. Malamataris et al. [4] observed changes in the tensile strength of tablets obtained from stored excipients at various environmental relative humidity by the combined effect of moisture on the intermolecular forces. Sun et al. [2] found that, under 3.3 wt.% water content, the compaction properties of MCC Avicel PH 102 were largely insensitive to moisture variation. Above 3.3 wt.% water content, the plasticity of the particle improved due to the plasticizing effect of water above the critical water content and a consequently larger interparticle bonding area when compressed. Hence, increasing moisture content also reduces bonding strength. Gregory E et al. [12] found that the powder flow of MCC PH101 decreases with increasing moisture content. The water acts as a plasticizer and influences the mechanical properties of MCC. The moisture content was also found (1) to affect the consolidation and compaction properties of the powder [13], and (2) to play a role in tablet delamination [14] and (3) punch sticking [15,16]. In more detail, these studies show that moisture plays an important role during the tablet compression process, since it affects the flowability and tabletability of the powder particles and contributes to several problems, such as tablet capping, tablet delamination, and punch sticking. Regarding the previous observations, it might become paramount to understand the powder particles' moisture behavior during compression.

The compaction process can be divided into two main stages. The first stage is the loading, where the powder is poured into the compression die and then compacted by applying a compression pressure on the powder particles with two punches (lower and upper). The second stage is the unloading, where the tablet is ejected from the die. To investigate the problems that occur during the compression, the loading stage is of high interest because, during this stage, the powder particles undergo plastic deformation, particle fragmentation, interparticle friction, and particle-wall friction [17–24], and the excess air in the interparticle pores escapes the compression die [25]. Hence, phenomena such as air entrapment [26], particle consolidation [25], and heat generation [19–24] were investigated during the loading phase of tableting. These phenomena are mainly investigated through modelling because of the difficulty of accessing the interior of the die during the loading phase [18–26].

However, there are no simulation studies on the behavior of the powder bed water content during compression [18–26]. Therefore, this work aims to present the first step toward the moisture behavior simulation by showing the methods that can be used to estimate the input parameters, which are the moisture transport coefficients. During the tableting process, the powder bed has a high porosity at the beginning of the compaction [2,27] and tends toward a very low porosity toward the end of the loading phase. Therefore, the powder bed can be modeled as a porous media with a pressure-dependent porosity to simulate the compactness evolution during the loading phase. In porous media, moisture diffuses in the form of water vapor through, mainly, the interparticle pores because of the combined action of: (1) capillary suction pressure (or partial water vapor pressure) [28–31] between the saturated powder's intraparticle pores and unsaturated interparticle air in the pores' network, (2) the vapor partial pressure gradient or relative humidity gradient between the interparticle pores and the ambient or surrounding air [29,30], and (3) the temperature gradient between the porous material and the surrounding air [29,30]. Simulation models based on Fick's and Darcy's [28] diffusion laws, and energy and mass conservation equations have been developed for saturated [29,31] and unsaturated hygroscopic porous media [32,33]. Hagentoft et al. [34] presented a benchmark-like model for heat, air, and moisture (HAM) analysis through porous materials. Their model was composed of a set of equations considering the temperature as potential for the energy conservation and the capillary suction pressure (or partial water vapor pressure) as potential of the moisture transport. Gerson Henrique et al. [30] derived a model which considers not a constant pressure of air in the porous material, but a transient air pressure.

In this study, we present novel methodologies to estimate the moisture coefficients, which are necessary to simulate the behavior of powder particles' moisture during the loading phase of the compression. The HAM model was adopted in this study. The modelling of relative humidity and water content distribution in the tablet during the loading phase of the compression process can be performed with commercial simulation software in which the HAM model is implemented, such as COMSOL Multiphysics®. Microcrystalline cellulose PH101 powder was used as the model powder material because it is widely used as an excipient in pharmaceutical formulation. The HAM model considers: (1) the deformation of the powder particles through the variation of the average porosity and heat production, (2) no advection due to buoyant force, even if an axial and high radial velocity of air was found in the powder bed during the tableting [35], (3) and no chemical reaction occurs during the loading phase.

1.1. Mathematical Model

At the beginning of the compression, the powder has the same temperature and relative humidity as it is surrounding environment, assuming an equilibrium state between the powder and the external environment. At standard temperature and pressure, the adsorbed layer on the surface and in the pores of the powder particle are in liquid mono, or multilayer states [36]. However, because the compression process is very fast and the powder has a low water content, the water is assumed to flow mainly in vapor form in high-velocity dry air [35,37], but the liquid form may still exist in the capillaries due to the hygroscopic powder particle. Hence, in the moisture transport equations, the liquid form of water is considered [30]. We assume that, during the compression, the moisture in both liquid and vapor forms diffuses through the interparticle pores, and the intraparticle diffusion is ignored. The heat produced during the compression, due to particle fragmentation, plastic deformation, interparticle friction, and die wall particle friction is assumed to interact with the absorbed layer of water. The mathematical model is described below. The pores and the water content are assumed to be homogeneous and well-distributed in the powder bed at the beginning of the loading phase. The tablet is assumed to be an isotropic porous material.

1.2. Heat Balance

During the compression, heat is generated from friction and particle deformation. The temperature space-time profile inside the powder bed can be calculated by means of heat balance equations:

$$(\rho C_p)_{eff} \frac{\partial(T)}{\partial t} + \nabla q = Q \quad (1)$$

$$q = -\lambda_{eff} \nabla T - L_v \delta_p \nabla(\varphi_w p_{sat}(T)) \quad (2)$$

where ρ is the effective density (kg/m^3), C_p is the specific heat at constant pressure (J/(kg·K)), λ is the thermal conductivity (W/(m·K)), L_v is the heat of evaporation (J/kg), and Q is the heat produced by friction and deformation (W/m^3).

The energy balance is applied to the considered porous media under the assumption of local thermodynamical equilibrium. In the first term of Equation (1), the effective thermal capacity is defined as follows:

$$(\rho C_p)_{eff} = \rho_s C_{p,s} + w C_{p,w} \quad (3)$$

1.3. Moisture Transport

The heat generated during the compression induces moisture gradients in the powder bed. The variation of the powder wetness during the compression can be obtained from the water mass conservation equation as [30,38,39]:

$$\frac{\partial(\varphi_w)}{\partial t} + \nabla g_w = G \quad (4)$$

with $g_w = -(\xi D_w \nabla \varphi_w + \delta_p \nabla(\varphi_w p_{sat}(T))$, and $\xi = \frac{\partial w(\varphi_w)}{\partial \varphi_w}$

$\xi D_w \nabla \varphi_w = D_w \frac{\partial w}{\partial \varphi} \nabla \varphi_w$ representing the vapor diffusion flux, and

$\delta_p \nabla(\varphi_w p_{sat}(T)) = \delta_p \nabla p_v(T)$ representing the capillary moisture flux;

φ_w is the relative humidity in the powder bed (%), δ_p is the vapor permeability (m^2/s), p_{sat} is the water vapor saturation pressure (Pa), p_v is the water partial vapor pressure (Pa), w is the moisture capacity (kg/kg), D_w is the moisture diffusivity (m/s^2), ξ is the water retention function (-), G is the generic moisture source representing the initial water content (kg/m^3), and T is the temperature (K).

Convective moisture transfer inside the powder bed and at the interface between powder bed and the compression tools was assumed and given by:

$$g_0 = -M_v h_m (C_{v,ext} - C_v) \quad (5)$$

with g_0 representing the moisture flow (m^2/s), M_v the molecular weight of water vapor (kg/mol), $C_{v,ext}$ the external vapor concentration (mol/m^3), and C_v the vapor concentration inside the tablet (mol/m^3); h_m is the moisture transfer coefficient (m/s).

Equations (4) and (5) are used to simulate the powder moisture profile and variation during the loading phase.

From the mathematical model, the moisture transport coefficients needed for the simulation are the vapor permeability (WVP), the moisture diffusion coefficient (MDC), and the moisture transfer coefficient (MTC). The next section presents the methods for estimating these coefficients.

2. Materials and Methods

2.1. Materials

MCC PH101 powder (Mallinckrodt Baker Inc., Phillipsburg, NJ, USA) was used in this study to make the tablets on which the measurements were made. The true density of the powder used in this study was 1550 kg/m^3 [2,27], and the loose bulk density measured

with a 100-mL graduated cylinder following the ASTM D7481-18 standard test method [40] was found to be 279.7 ± 2.5 kg/m^3.

2.2. Methods

2.2.1. Powder Particles' Water Content

The water content of the powder particle was measured with a high-precision balance equipped with an infrared heater, the Mettler PM 100 apparatus (Mettler-Toledo Ltd., Leicester, UK). It dries the powder with an infrared source and calculates the water content by mass difference. The mean of three measurements was calculated; the value obtained for the powder moisture content was 3.2 wt.% at a relative humidity of 38% and temperature of 25 °C.

2.2.2. Powder Particles' Size Distribution

The powder particles' size range was measured by the sieving method with a Gilson Sieve Shaker SS-8R and SS-12R (Gilson Company, Inc., Lewis Center, OH, USA). The size of the particles was controlled by mechanical screening via the use of a vibrating sieve (Gilson Sieve Shaker, SS-8R), employing the screens of 150 µm and 90 µm for a sifting time of 20 min. The powder size distribution used in this study ranged from 90 µm to 150 µm.

2.2.3. Tablet Compression

The powder was compressed on a CARVER 12-ton manual hydraulic press in an environment of 38% relative humidity and a temperature of 25 °C. A 5.6-g MCC PH101 powder sample was compressed in a stainless-steel 304 die (25 mm in diameter), with a compression pressure from 20 MPa to 200 MPa applied with a 304 stainless-steel flat-face punch set. The powder was poured into the compression die manually in the compression just after weighing the powder. The relative density of the obtained tablets at every compression pressure is calculated with Equation (6) [41]:

$$RD = \frac{\rho_{app}}{\rho_{true}} = \frac{m}{V} \times \left(\frac{1}{\rho_{true}}\right), \ \ were\ V = \pi r^2 L \tag{6}$$

where ρ_{app} is the apparent density of the compressed tablet (kg/m^3), ρ_{true} is the dry solid particle true density (kg/m^3), m is the compressed powder tablet mass (kg), V is the compressed powder tablet volume (m^3), r is the radius of the compressed powder tablet (m), and L is the thickness of the compressed powder tablet (m).

The tablet porosity was estimated from the tablet relative density with the Equation (7) [2,27]:

$$\varepsilon = 1 - RD = 1 - \frac{\rho_{app}}{\rho_{true}} \tag{7}$$

where ε is the tablet average porosity (-).

2.2.4. Particle and Compressed Powder Tablet Surface Analysis

The tablet surface features were imaged with scanning electron microscopy (SEM) (S-4700, Hitachi America, Ltd., Santa Clara, CA, USA) in BSE (backscattering) mode with, respectively, 20-kV acceleration tension at a working distance of 9.7 mm. Tablets obtained at 200 MPa were used as samples.

2.2.5. Tablet Internal Pore Size Distribution

The internal pore size distribution in the compressed tablet at different relative densities is measured. The water droplet penetration time method was used to estimate the pore size in the compressed powder tablet.

Water Penetration Time Method

Imbibition of a single drop into a porous substrate depends on the structure of the substrate: the porosity, the size of the pores, the orientation of the pores, and the surface chemistry within the compacted bed [42]. When a porous material is easily wetted by a fluid, that is, when the contact angle between the fluid and the material is less than 90°, the penetration of the fluid into the material pores will begin to occur due to the capillary suction. The rate at which a single drop of fluid with volume V_d, viscosity μ, and surface tension γ_{lv} penetrates a static porous medium, as a compact powder bed, with cylindrical pores of R_{pore} and an overall porosity of ε, is given by the drop penetration time t_p [43]. By modeling the pores in the porous material as a bundle of vertical, parallel, cylindrical, and randomly distributed capillaries, we can estimate the average pore radius in the porous material with Equation (8) [42]:

$$t_p = 1.35 \times \frac{V_d^{\frac{2}{3}}}{\varepsilon^2 R_{pore}} \times \frac{\mu}{\gamma_{lv} \cos\theta} \quad (8)$$

where t_p represents the penetration time of the droplet into the porous material (s), V_d is the droplet volume (m^3), ε is the average porosity of the tablet (-), R_{pore} represents the average pore radius of the tablet (m), θ is the static contact angle between the tablet and the water droplet (°), γ_{lv} is the water surface tension (J/m^2), and μ is the dynamic water viscosity (Pa·s).

The penetration time of a droplet of water of volume 2 µL deposited at the top of the compressed tablet, at a rate of 2.67 µL/s, was measured by using a drop shape analyzer (DSA25, KRÜSS, Matthews, NC, USA), equipped with a high-speed camera and a humidity chamber where the temperature can be controlled (Figure 1). A 500-µL syringe with a 24−gauge needle was used to deliver precisely 2-µL droplets at 5-mm height to avoid splashing. The penetration process, from the contact between the droplet and the substrate surface to the total penetration of the droplet, was recorded at a high frame rate of 350 fps. The video was recorded and analyzed with the ADVANCE software attached to the KRÜSS® apparatus. The measurements were done on a compressed powder tablet produced with different compression pressures ranging from 20 MPa to 200 MPa. For each trial, one droplet was deposited at the surface of the tablet, and three replicates were done for each compression pressure.

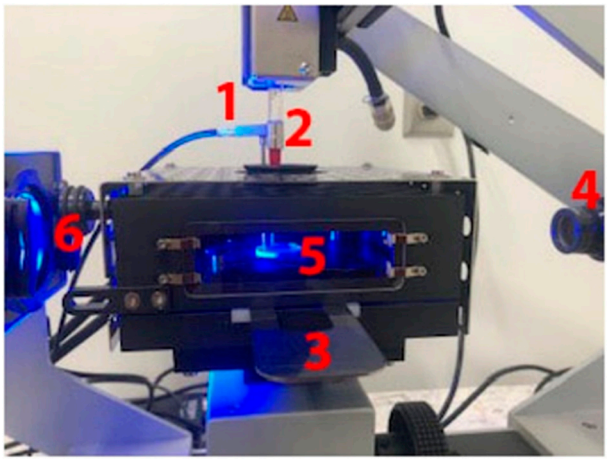

Figure 1. Drop shape analyzer used for static contact angle and penetration time measurement. (1): temperature probe, (2): 500 µL syringe, (3): compressed powder holder, (4): high-speed camera, (5): temperature- and humidity-controlled chamber, (6): light source. Image take from KRÜSS® drop shape analyzer.

The same apparatus was used to measure the static contact angle between the water droplet and compressed tablets obtained at high compression pressure (200 MPa).

2.2.6. Moisture Transport Coefficient Determination Methods

Tablet Moisture Transfer Coefficient (ASTM D6539)

The moisture transfer coefficient (MTC) of a material is usually measured with the dry cup technique based on the ASTM E96 method [44]. Because the dry cup technique is not quick enough to limit the swelling effect of the powder particle in the tablet, this method was not used in this study. Instead, inert gas permeability was measured based on ASTM D6539 [45] standards to measure the gas permeability of the compressed powder tablet (Figure 2). The so-obtained permeability value can be used to estimate the hydraulic conductivity of the compressed powder tablet, which was adopted as the moisture transfer coefficient.

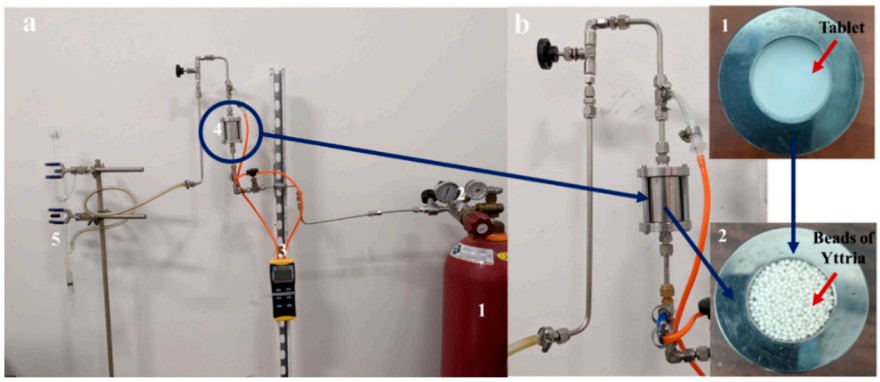

Figure 2. (**a**) Setup for gas permeability measurement in an MCC PH101 tablet. (**b**) Picture showing the (**b1**) tablet in the die and (**b2**) the yttria beads used to fill the die on top of the tablet.

The setup (Figure 2a) is composed of a helium gas bottle, a regulator (1 in Figure 2a), an inlet pressure gage (0–100 psi) (2 in Figure 2a), a differential pressure gage (0 to 100 psi) (3 in Figure 2a), a sealed die that contains the compressed powder tablet (4 in Figure 2a), and a bubble meter for the outflow measurement (5 in Figure 2a). The compressed powder tablet was left in the die after compression to ensure no gap existed between the die wall and the peripheral surface of the tablet (1 in Figure 2b). Small beads of yttria were used to fill the die on top of the tablet (Figure 2b2). Before the test, the tablet stability inside the die was tested with the required test pressure (5 psi to 35 psi). The measurements were done on tablets obtained with 60 MPa, 100 MPa, 140 MPa, and 200 MPa. Four replicates were recorded for each inlet gas pressure.

Tablet Moisture Diffusion Coefficient

The water vapor diffuses through three different diffusion regimes. The ordinary diffusion is governed by a collision between diffusing molecules, the free molecular or Knudsen diffusion, and the transient diffusion regime. The main diffusion mechanism by which the vapor diffuses through the tablet can be obtained by using the Knudsen number (Equation (9)), which is the ratio of the mean free path of the water vapor to the tablet pore radius [29,46]:

$$K_n = \frac{\lambda}{r_0} \tag{9}$$

where λ is the mean free path (m), r_0 is the average pore radius (m), and K_n is the Knudsen number (-).

1. When $K_n < 0.01$, the water vapor follows a continuum flow. The mean free path of the water vapor molecules is much less than the pore's radius, which means that particle–

particle collision dominates the diffusion in the compressed powder tablet pore. The diffusion coefficient is then estimated by the classical molecular diffusion D_0.

2. When $0.1 < K_n < 10$, the water vapor follows a transitional flow. The diffusion is a mixture of particle−particle collisions and particle−wall collisions. In that case, the diffusion coefficient is given by [43]:

$$\frac{1}{D_{trans}} = \frac{1}{D_k} + \frac{1}{D_0} \tag{10}$$

where D_{trans} is the transitional diffusion coefficient (m^2/s), and D_k is the Knudsen diffusion coefficient (m^2/s).

3. When $Kn > 10$, the water vapor follows the free molecular flow, which is also called Knudsen diffusion. The mean free path of the water vapor molecules is greater than the pore radius. Molecule–pore wall collisions dominate the water vapor diffusion in the compressed powder tablet pore. The diffusion coefficient is given by [43,46]:

$$D_k = \frac{8r}{3}\left(\frac{RT}{2\pi M}\right)^{0.5} \tag{11}$$

where D_k is the Knudsen diffusion coefficient (m^2/s), R is the gas constant (J/(K·mol)), T is the temperature (K), r is the pore radius (m), and M is the molecular mass of the diffusing species (kg/mol).

The mean free path of travel (λ) refers to the distance between molecular collisions and can be estimated using Equation (12) [47]:

$$\lambda = \frac{\mu}{P}\sqrt{\frac{\pi RT}{2M}} \tag{12}$$

where λ is the mean free path of the water molecules in the pores (m), μ is the dynamic viscosity of the fluid (Pa·s), R is the gas constant (J/(K·mol)), M is the molecular weight (kg/mol), P is the diffusion species pressure (Pa), and T is the tablet temperature (K).

Water Vapor Permeability

Woodside [48] deduced a theoretical expression for the water vapor permeability (WVP) coefficient expression for an unsaturated porous media by using the law of heat conduction (7). The theoretical expression agrees with the empirical relationships found by Penman and Edenholm for soils, glass spheres, charcoal, and cellular concrete [49,50]. Water vapor was evaporated and forced to pass through a bed of soil and concrete pellets to measure the WVP on soils and concrete experimentally [50].

Because of the hygroscopic property of microcrystalline cellulose, water vapor was not ideal for this study. Microcrystalline cellulose particles swell in contact with moisture, and the increase of the size of the particles will plug the interparticle pores of the pellet and skew the result of the permeability measurement [51]. Hence, the Woodside expression was used in this study to estimate the (WVP) based on the (WVP) in air [48]:

$$\frac{\mu}{\mu_{air}} = \frac{2\varepsilon}{3-\varepsilon} \tag{13}$$

where μ represents WVP in the compressed powder tablet (s), μ_{air} is the WVP in air at room temperature equal to 0.069 kg/m × atm × h (1.91667×10^{-10} s) [48], and ε is the compressed powder tablet porosity (-).

Quenard and Sallée (QS) [52] also derived a model to estimate the WVP for porous material-based capillary network methods, where the flux of the water must be described by a Fick-like law. Assuming no capillary condensation, the WVP was given by:

$$K_v = \frac{M}{RT}\left(\frac{D}{1+\frac{L_m}{2R_p}}\right) \quad (14)$$

where D is the water diffusive coefficient (WDC) (m^2/s), L_m is the mean free path of the water molecule (m), M is the molecular weight of water molecule (kg/mol), T is the temperature (K), R is the gas constant (J/(K·mol)) and Rp is the pore radius (m).

The QS model is valid for molecular diffusion and Knudsen diffusion.

3. Results

3.1. Tablet Relative Density and Porosity

The compactness (the relative density or the porosity) of the compressed powder tablet was calculated at each compression pressure, from 20 MPa to 200 MPa. Table 1 shows the relative density and porosity values obtained from the measured thickness and radius of the compressed powder tablet.

Table 1. Relative density for compressed powder tablets obtained at each compression pressure.

P ($\times 10^6$ Pa)	L ($\times 10^{-3}$ m)	R ($\times 10^{-2}$ m)	V ($\times 10^{-6}$ m^3)	ρ_{app} (kg/m^3)	ρ_{true} (kg/m^3)	RD (-)	ε (-)
LP	-	-	-	279 (4.15)		0.18 (0.01)	0.82 (0.01)
20	10.21 (0.25)		5.16 (0.12)	1074.41 (2.65)		0.69 (0.02)	0.31 (0.0)
40	9.70 (0.20)		4.91 (0.10)	1142.31 (3.45)		0.74 (0.02)	0.26 (0.0)
60	9.31 (0.23)		4.71 (0.05)	1192.15 (2.16)		0.77 (0.02)	0.23 (0.0)
80	8.97 (0.17)		4.54 (0.09)	1230.27 (3.05)		0.79 (0.02)	0.21 (0.0)
100	8.63 (0.10)	1.25 (0.04)	4.37 (0.12)	1282.71 (1.97)	1550 (15)	0.83 (0.02)	0.17 (0.0)
120	8.44 (0.14)		4.27 (0.08)	1309.82 (1.65)		0.84 (0.02)	0.16 (0.0)
140	8.06 (0.11)		4.08 (0.07)	1373.60 (4.20)		0.89 (0.02)	0.11 (0.0)
160	7.94 (0.07)		4.02 (0.03)	1395.32 (3.71)		0.90 (0.02)	0.10 (0.0)
180	7.93 (0.09)		4.02 (0.06)	1409.12 (4.45)		0.91 (0.02)	0.09 (0.0)
200	7.64 (0.10)		3.87 (0.04)	1447.21 (2.07)		0.93 (0.02)	0.07 (0.0)

LP: Loose Powder, Error at 68.2% of confidence interval in brackets.

The porosity (Figure 3a) and the relative density (Figure 3b) of the compressed powder tablet increases and decreases, respectively, with the compression pressure, and tends to stabilize at high compression pressures. During the compression, the plastic deformation of the MCC particles creates more interacting surfaces. A large part of the air inside the pore escapes the powder bed, leaving the particles to draw nearer with the increase of the compression pressure. Consequently, the overall porosity decreases (the relative density increases) in the powder bed. At higher pressures, the adjacent particles deformed locally to adapt to each other without impacting the porosity (relative density) of the obtained tablet [2]. Thus, this can explain the steady state observed at low porosity (high relative density). By increasing the compression pressure, the rate of deformation increases, leading to closer particles, a higher density of particles per volume unit, and hence, higher compactness and less porosity. The same results were observed during the compression of a microcrystalline cellulose PH102 powder [5].

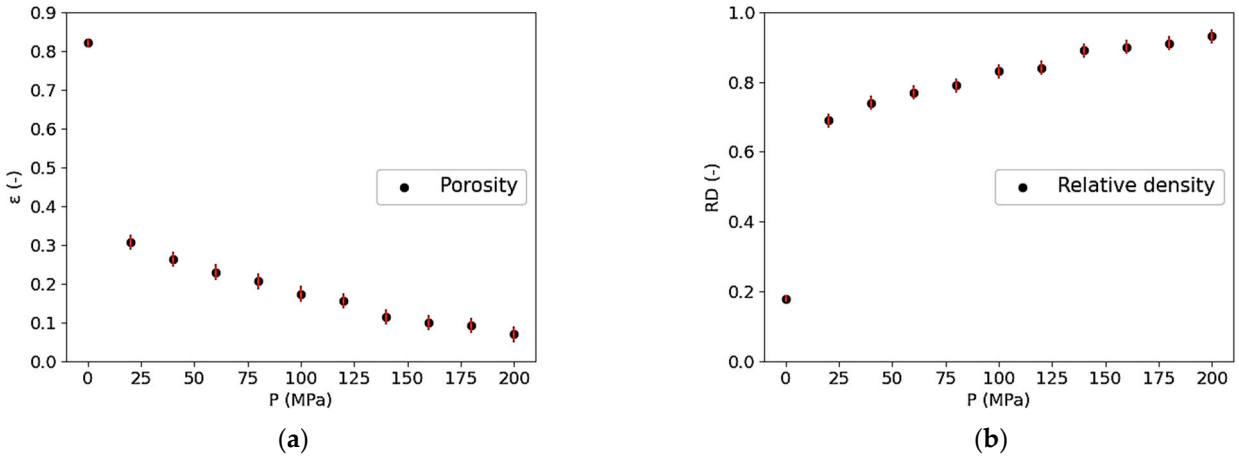

Figure 3. MCC PH101 tablet (**a**) average porosity and (**b**) relative density variation with the compression pressure.

3.2. Tablet Average Pore Radius at Each Compression Pressure

Large and small interparticle pores are non-homogeneously distributed at the tablet surface, which is not ideal for determining an average pore radius value (Figure 4). Therefore, we used the penetration time method to estimate the average pore radius. This method of measurement depends on the contact angle between the water droplet and the compressed powder tablet. The water droplet at the top of the tablet surface must be stable with a well-defined hemisphere shape. Because the stability of the droplet depends on the capillary suction of the droplet into the pores, the measurement must be done at very low porosity. Therefore, a tablet obtained at 200 MPa was used to measure the contact angle. A value of 41° ± 3.5° (Figure 5) was obtained from a mean value of three replicates, which corroborates the hydrophilic nature of the MCC PH101 [31]. The same contact angle value was used for the tablets obtained at lower compression pressures since it is the same material.

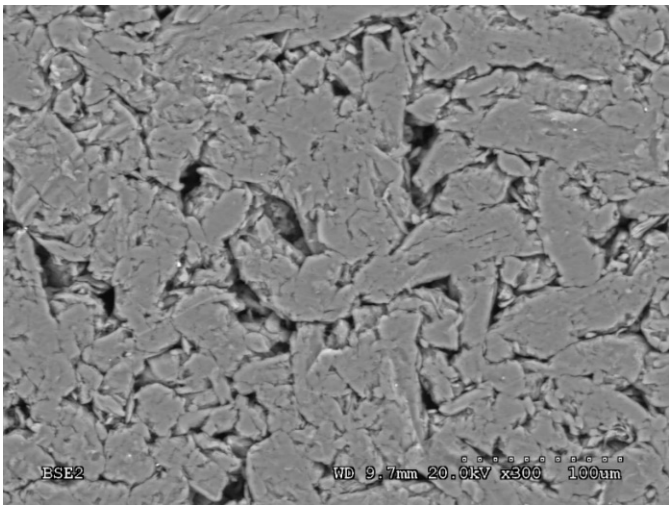

Figure 4. Surface pores' structure of a tablet at 90% of relative density (10% porosity) of the compressed powder tablet. Image obtained via scanning electron microscopy (SEM) (S-4700, Hitachi America, Ltd., Santa Clara, CA, USA) in BSE (backscattering) mode with, respectively, 20-kV acceleration tension at a working distance of 9.7 mm.

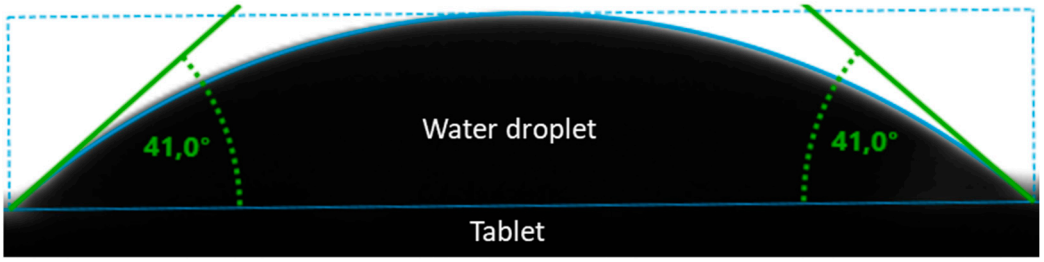

Figure 5. Contact angle between the compressed powder tablet (200 MP) and the water droplet. Image obtained with KRÜSS ADVANCE software. A 2-µL water droplet was placed on a MCC tablet surface compressed with a 200-MPa compression pressure.

After the penetration of the droplet, the particles at the tablet surface swelled (Figures 6 and 7). This observation is more obvious on the tablet produced with a compression pressure of 200 MPa (Figure 7e) because the droplet residence time at the top surface of the tablet is longer. However, for the tablet compressed at a compression pressure of 20 MPa, the particles swell a few seconds after the penetration (Figure 6h). The swelling effect can be considered to take place after the interparticle pores are filled with water; hence, the water diffuses through the intraparticle pores. Because the interparticle pores in the less compacted tablet can be considered to be wider, the penetration time can be fully attributed to the water diffusion through the interparticle pores. Thus, in the case of the highly compacted tablet, the penetration time depends upon a combination of the water diffusing through the interparticle and intraparticle pores. Because of the swelling effect, the stability of the measured pores' average radius with the water droplet penetration method must be further investigated.

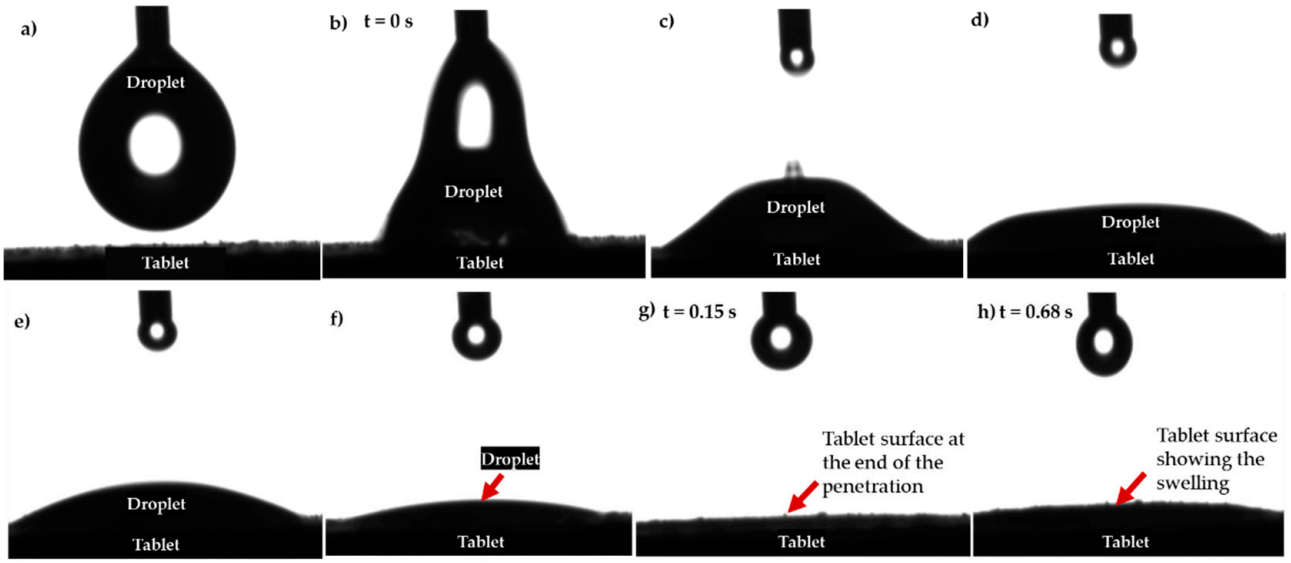

Figure 6. Series of images showing (**a**) the water droplet at the tip of the needle and the tablet surface, (**b**) the contact between the surface and the droplet, (**c**) the beginning of the penetration, (**d**–**f**) the intermediate stage of the penetration, (**g**) the end of the penetration, and (**h**) the swelling of the particle after the penetration. The tablet was compressed at 20 MPa.

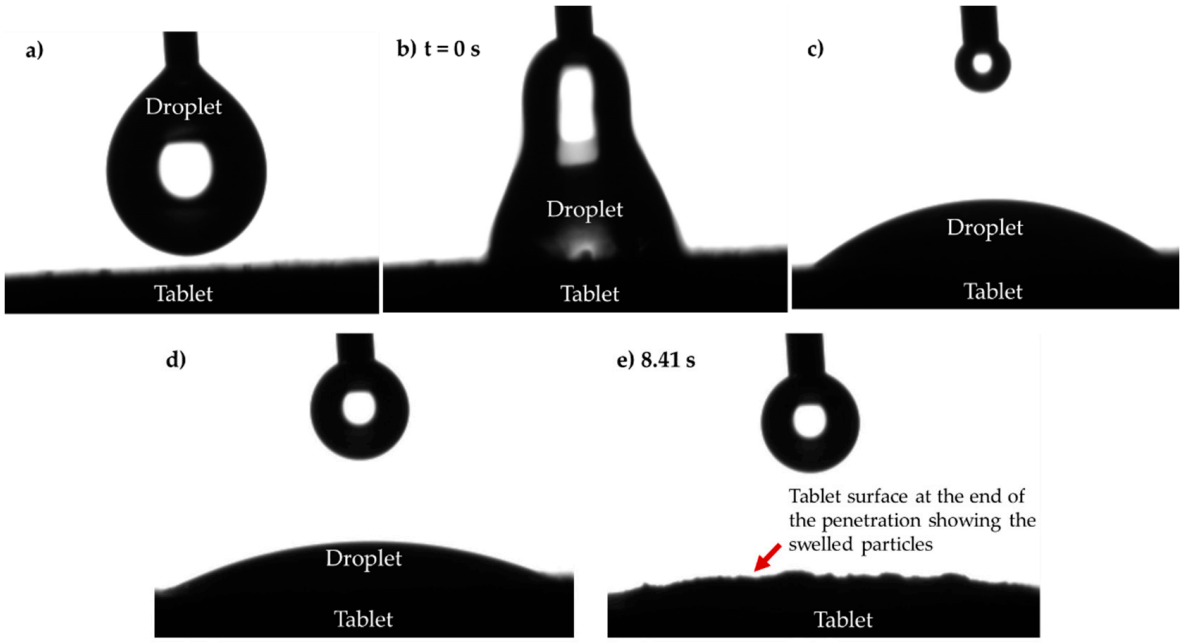

Figure 7. Series of images showing (**a**) the water droplet at the tip of the needle and the tablet surface, (**b**) the contact between the tablet surface and the droplet, (**c**–**d**) the penetration, and (**e**) the end of the penetration and the swelling of the particle after the penetration. The tablet was compressed at 200 MPa.

Table 2 lists the mean penetration time measured for the compressed powder tablet produced with compression pressures ranging from 20 MPa to 200 MPa. The calculated average (Equation (8)) pore radius for each compression pressure is also shown.

Table 2. Measured water droplet penetration time and calculated pore radius values.

P ($\times 10^6$ Pa)	tp (s)	Θ (°)	γ ($\times 10^{-2}$ j/m^2)	V_d ($\times 10^{-9}$ m^3)	RD (-)	ε (-)	μ ($\times 10^{-3}$ Pa·s)	r ($\times 10^{-6}$ m)
20	0.15 (0.00)	41 (3.5)	7.20	2.0 (0.6)	0.69 (0.02)	0.31 (0.0)	1	2.83 (0.05)
40	0.45 (0.03)				0.74 (0.02)	0.26 (0.0)	1	1.25 (0.05)
60	0.72 (0.07)				0.77 (0.02)	0.23 (0.0)	1	1.03 (0.06)
80	1.29 (0.03)				0.79 (0.02)	0.21 (0.0)	1	0.76 (0.01)
100	1.70 (0.07)				0.83 (0.02)	0.17 (0.0)	1	0.75 (0.02)
120	2.78 (0.26)				0.84 (0.02)	0.16 (0.0)	1	0.68 (0.05)
140	3.88 (0.19)				0.89 (0.02)	0.11 (0.0)	1	0.76 (0.02)
160	4.58 (0.40)				0.90 (0.02)	0.10 (0.0)	1	0.69 (0.04)
180	6.34 (0.51)				0.91 (0.02)	0.09 (0.0)	1	0.72 (0.03)
200	8.48 (0.59)				0.93 (0.02)	0.07 (0.0)	1	0.74 (0.04)

Error at 68.2% of confidence interval (in brackets).

The average pore radii of MCC compressed powder tablets obtained from the water droplet penetration time method range between 0.57 µm and 2.8 µm. The pore size distribution measured with the mercury porosimetry method [53] on an MCC Avicel PH101 compressed powder tablet with the same compactness as in this study was found to range between 0.5 µm and 2 µm, which is in agreement with our results. Additionally, a numerical method [46] used to estimate the interparticle average pore radius of MCC PH102 tablet with a relative density of 90% gave a result of 6.3 µm, which is not far away from our result. The observed discrepancy between our result and the later method can be due to the difference in the true density of the powder used and the initial moisture content of the powder before the compression. Therefore, the values of the pores' radii obtained in this study were used to calculate the moisture transport coefficient.

Figure 8a,b show, respectively, the variation of the average tablet pore size and the penetration time with the relative density. The water droplet penetration time increases with

the compactness due to the decrease of the pore radius and the porosity. The penetration of the water droplet in the tablet is due to the capillary suction inside the interparticle pores of the tablet. At higher porosities and for larger pores, the acting capillary pressure gradient on the droplet is strong and tends to increase the capillary suction and decrease the water droplet penetration time. The decrease of the interparticle pore radius and the tablet average porosity weakens the capillary pressure gradient, hence the increase of the penetration [42,54,55].

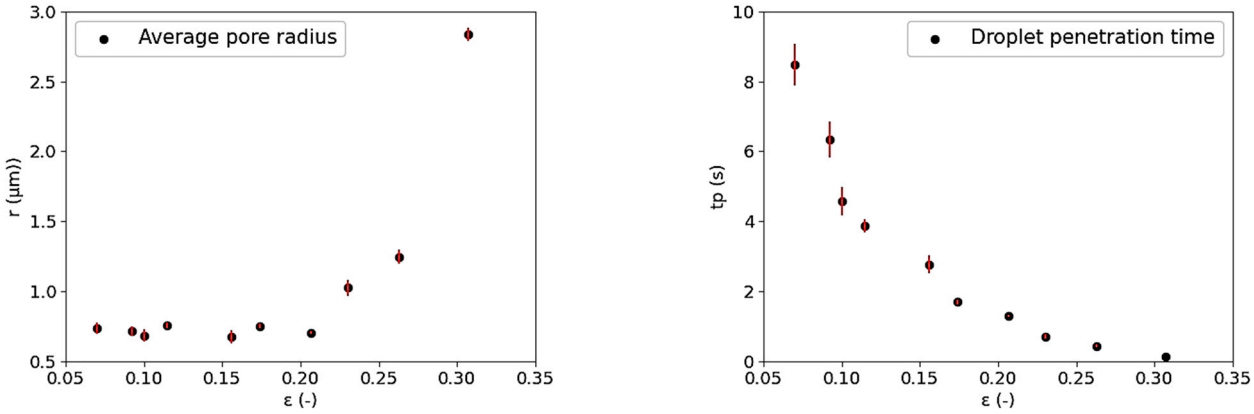

(**a**) (**b**)

Figure 8. Variation of (**a**) the average pore radius and (**b**) the water droplet penetration time with the compressed MCC PH101 powder tablet average porosity.

The pore radius decreases abruptly between a porosity of 30% and 15% in the low compression pressure region and stabilizes at the lowest porosity, where it reaches a minimum value. Because increasing the compaction pressure induces a higher plastic deformation rate for the particle, the interparticle space becomes smaller [27]. Below 15%, the steady state observed can be explained by the local deformation, without expansion, of the adjacent particles to adapt to each other [2].

3.3. Tablet Moisture Transfer Coefficient (ASTM D6539)

A mean value for the outflow was calculated from four replicates of values measured with the bubble meter for each compressed powder tablet at every gas pressure, ranging from 5 psi to 35 psi, with a pressure increase of 5 psi. Each trial was made on a compressed powder tablet produced with compression pressure of 60 MPa, 100 MPa, 140 MPa, and 200 MPa, respectively. The average value of the outflow was used to calculate the average outflow (Equation (15)) at the center of the tablet by considering a linear distribution of the flow in the tablet. The results of the measured outflows and the average outflows for the compressed powder tablet at each compression pressure are reported in Table S1 of the supplementary data. A *t*-test between the measured outflow of each tablet at the same inlet pressure gives a value of $p >> 0.05$, which means that the measured outflows are not statistically different. The measurements for tablets obtained at 60 MPa are stopped at a gas inlet pressure of 15 psi, because that is the critical pressure that the tablet can handle.

$$Q_{av} = Q \times \frac{P_B}{P_I + P_B - \frac{\Delta P}{2}} \quad (15)$$

Q_{av} is the average outflow at the center of the tablet (m^3/s), Q is the measured outflow (m^3/s), P_I is the entry gas gage pressure (Pa), P_B is the barometric pressure (Pa), and ΔP is the differential pressure across the tablet (Pa).

ASTM D6539 states that all the obtained values of average flow must lie in the laminar domain (domain between the upper (+25% Q_{av}) and lower limit (−25% Q_{av})) before using

them for the permeability determination. All values outside the laminar domain must be rejected. Figure 9a–h show the obtained average outflow values.

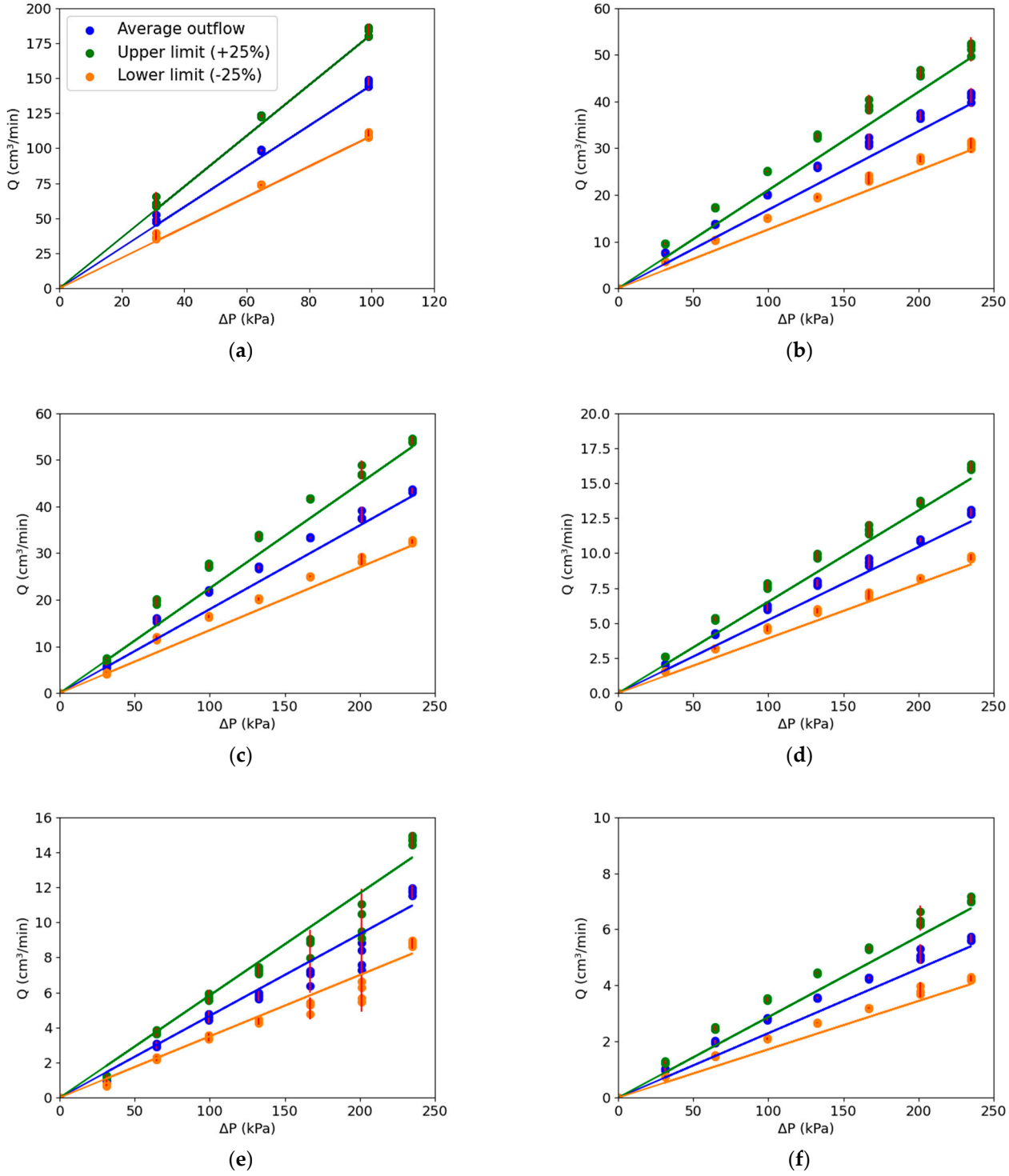

Figure 9. *Cont.*

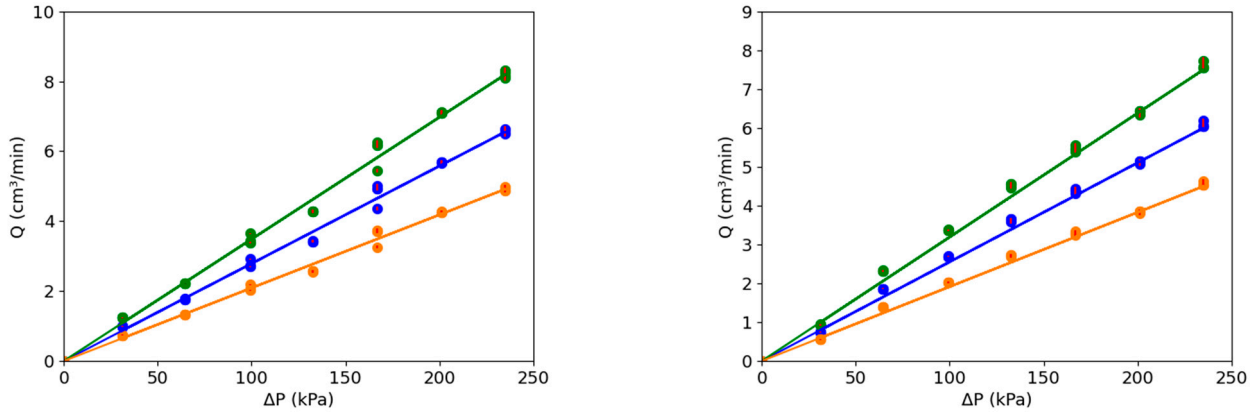

Figure 9. The average outflow versus the pressure drops across MCC PH101 tablets obtained at (**a**) 60 MPa, (**b**) 80 MPa, (**c**) 100 MPa, (**d**) 120 MPa, (**e**) 140 MPa, (**f**) 160 MPa, (**g**) 180 MPa, and (**h**) 200 MPa. The laminar domain is between the upper (+25%) and lower limit (−25%).

The measured average outflows, which were in the laminar domain for all compressed powder tablets (obtained at 60 MPa, 80 MPa, 100 MPa, 120 MPa, 140 MPa, 160 MPa, 180 MPa, and 200 MPa), were used to estimate the permeability.

The Darcy permeability *Kp* is given by Equation (16) [45]:

$$K_p = \frac{Q_{AV}}{\Delta P} \times \frac{L}{A} \times \mu \times 1.1013 \times 10^{12} \quad (16)$$

where K_p is the permeability (Darcy), Q_{AV} is the average outflow (m^3/s), L is the thickness of the tablet (m), A is the tablet cross-section (m^2), ΔP is the pressure drop across the specimen (Pa), and μ is the viscosity of the gas at the test temperature (Pa·s).

Because all the values of the average outflow measured at each inlet gas pressure are in the laminar domain and are not statistically different ($p_{value} > 0.05$), their average values were used to calculate the tablet permeability (See Table S2 in Supplementary Data for the obtained values of the permeability at each compression pressure).

The permeability values obtained from the measurements on tablets compressed at the same pressure are in the same range for each tablet, regardless of the inlet gas pressure. Hence, the variation of the permeability with the tablet porosity (compactness) can be determined by using the mean value of the permeability for each compression pressure. Table 3 reports the measured mean permeability values.

Table 3. Mean permeability values for each compressed powder tablet porosity.

P ($\times 10^6$ Pa)	RD (-)	ε (-)	*Kp* ($\times 10^{-16}$ m^2)
60	0.77 (0.02)	0.23 (0.0)	97.6 (0.6)
80	0.79 (0.02)	0.21 (0.0)	12.3 (0.1)
100	0.83 (0.02)	0.17 (0.0)	12 (0.1)
120	0.85 (0.02)	0.15 (0.0)	3.47 (0.01)
140	0.89 (0.02)	0.11 (0.0)	2.36 (0.01)
160	0.90 (0.02)	0.10 (0.0)	1.54 (0.02)
180	0.91 (0.02)	0.09 (0.0)	1.50 (0.01)
200	0.93 (0.02)	0.07 (0.0)	1.39 (0.01)

Error at 68.2% of confidence interval (in brackets).

Very low permeability values are obtained at each compressed tablet compactness. This is attributed to the very low porosity and the micrometric pore radius of the tablets [56]. The permeability in porous media can be predicted using the Kozeny–Carmen (KC) equation [28,56,57], $Kp = \frac{\varepsilon^3}{c(1-\varepsilon)^2 S^2}$, where ε is the porous material porosity, S, the function of the

tortuosity, is the specific surface area based on the volume, and c is the KC constant. Many semi-empirical models based on the KC equation have been developed in past years where a constant, B, and the tortuosity of pores' channels is used to fit the measured values of permeability, $Kp = B\frac{\varepsilon^3}{\tau^2 S^2}$ [57]; other models were developed based on: (1) the material particle average size, d, $Kp = \frac{\varepsilon^3}{k(1-\varepsilon)^2}d^2$ [29,58], and (2) pore radius $Kp = \frac{g\times\varepsilon}{800}r^2$ [59]. The pores network inside the porous material was described with the fractal pore space geometry assumption [60–62], which leads to a fractal-based model function of (1) only the porosity and the empirical constants, n, C, and $Kp = C\frac{\varepsilon^{n+1}}{(1-\varepsilon)^n}$ [63], and (2) the pore radius, λ, the porosity, and a fractal constant, D_f, for straight capillary pores $Kp = \frac{(2-D_f)}{32(4-D_f)}\left(\frac{\varepsilon}{1-\varepsilon}\right) \times \lambda^{\,2}_{max}$ [57], where, $1 < D_f < 2$ and $2 < D_f < 3$ respectively for two- and three-dimensional fractal pore spaces, respectively. Because the size of the particle during the compaction can change due to deformation and fragmentation [64], the models using pore radius and porosity are used in this study to predict our measurement. We assumed in our study that the permeability is proportional to the square of the pore radius, as below:

$$Kp = \beta(\varepsilon) \times r^2 \tag{17}$$

where $\beta(\varepsilon)$ is a parameter function of the porosity in the tablet at each compression stage. Table 3 shows the values of permeability measured in this study. The measured radius with the time penetration method was used to predict the permeability measured. The porosity-dependent parameter was obtained by fitting the measured values with Equation (17). Figure 8 shows the variation of the permeability with the tablet average porosity. Traxel and Baum's [59] and Xu and Yu's [57] models predicted an overall permeability value in the same range as the measured values. However, above a porosity of 18%, the values were underestimated. Nevertheless, these results show that the permeability of the tablets can be predicted with the well-known values of the tablet average porosity and pore radius. Our model, shown in Equation (18), predicts the measured permeability well, with a $R^2 = 0.983$:

$$Kp = 0.707(\varepsilon)^3 \times r^2 \; with \;\; \beta(\phi) = 0.707(\varepsilon)^3 \tag{18}$$

where Kp is the permeability (m^2), ε is the average porosity (-), and r represents the average pore radius (m). The constant value 0.707 in the parameter β(ε), according to Carman [28], corresponds to the inverse of the tortuosity, $\frac{1}{\tau} = \frac{L}{L_e} = \frac{1}{\sqrt{2}}$. L is the apparent flow path length of the diffusing molecules, which represents the porous material thickness, assuming a bundle of vertical cylindric capillaries, and L_e is the effective path length of the diffusion molecules. Consequently, our model can be written as below:

$$Kp = \frac{1}{\tau}(\varepsilon)^3 \times r^2 with\ \tau = \frac{L_e}{L} = \sqrt{2} \tag{19}$$

This model links the microstructural characteristics of the tablet (tortuosity, the interparticle average pore, and the average porosity) to the measured permeability, and follows the well-known Carman–Kozeny model. At the same time, our model is very simple and can be useful to estimate the permeability from the average value of the compressed tablets' interparticle pores and vice versa.

The tablet permeability decreases with the porosity (Figure 10) and reaches a steady state at a porosity around 11%. From the first partial derivative of our model (Equation (20)), the porosity variation was found to be the main microstructural feature that impacts the variation of the permeability ($3\varepsilon^2 r^2 d\varepsilon > 2\varepsilon^3 rdr$). Thus, the decrease of the permeability can be due to the plastic deformation of MCC soft particles, which close the pores in the tablet, leading to a decrease in the overall porosity of the tablet [2,5]. When the compression pressure increases, the tablet becomes more compact and, at certain pressures, the adjacent particles deform locally to conform to each other without affecting the porosity [5]; this can explain the steady state reached at very low porosity (<0.11) [57,64]. With the range of

permeability values measured, the compressed MCC PH101 powder tablet can be classified as a semi-pervious material [28]:

$$dK_p = \frac{1}{\tau}\left(3(\varepsilon)^2 \times r^2 d\varepsilon + 2(\varepsilon)^2 r dr\right),\ with\ \tau = cste \tag{20}$$

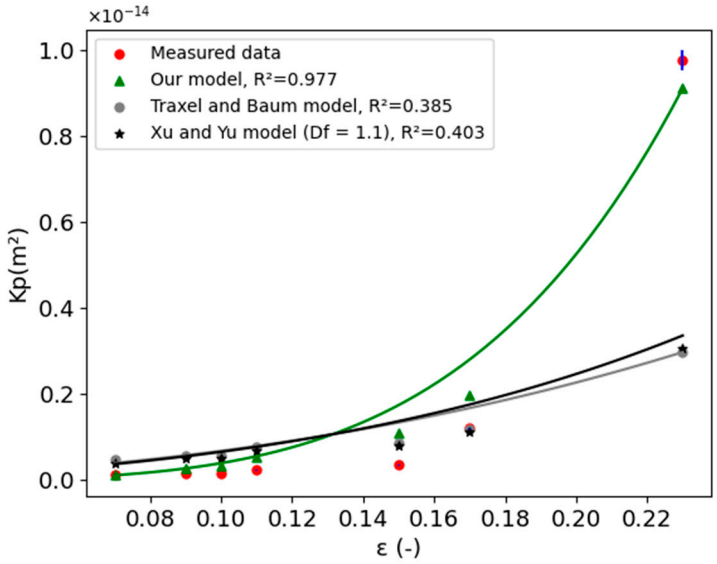

Figure 10. Variation of the permeability with the compressed MCC PH101 powder tablet porosity.

For simulation purposes, the measured data was fitted with a normalized exponential equation (Figure 11). The fitted equation (Equation (21)) can be implemented in a COMSOL Multiphysics® HAM model to define the permeability of the MCC PH101 tablet function of the porosity or the relative density. The same exponential fit was found between a normalized permeability of compacted spheres and a normalized compaction pressure [64]:

$$\frac{K_p}{K_{p0}} = 2.53 \times 10^{-4} \exp\left(\frac{8.28 \times \varepsilon}{\varepsilon_0}\right) \tag{21}$$

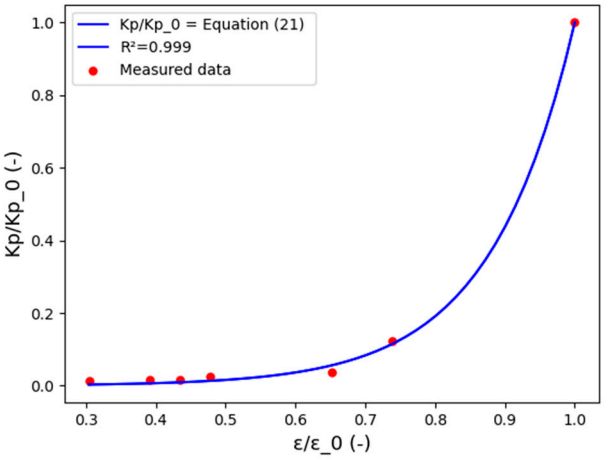

Figure 11. Variation of the measured permeability with the compressed MCC PH101 powder tablet porosity.

From the measured permeability, the hydraulic conductivity, which represents the MTC of the compressed tablet obtained at each compression pressure, was estimated with Equation (22) [43]:

$$K = \frac{K_p \rho g}{\mu} \tag{22}$$

where K represents the hydraulic conductivity (m/s), Kp is the Darcy permeability (m^2), g is the standard gravitational acceleration (m/s^2), and μ is the gas viscosity (Pa·s).

Table 4 shows the hydraulic conductivity calculated for each compressed powder tablet at different relative densities.

Table 4. Hydraulic conductivity calculated with helium properties.

P ($\times 10^6$ Pa)	RD (-)	ε (-)	Kp ($\times 10^{-16}$ m^2)	μ ($\times 10^{-5}$ Pa·s) [65]	g (m/s^2)	ρ (kg/m^3) [66]	K ($\times 10^{-11}$ m/s)
60	0.77 (0.02)	0.23 (0.0)	97.6 (0.6)	1.99	9.8	0.17	80 (0.5)
80	0.79 (0.02)	0.21 (0.0)	12.3 (0.1)				10.10 (0.10)
100	0.83 (0.02)	0.17 (0.0)	12 (0.1)				9.87 (0.10)
120	0.85 (0.02)	0.15 (0.0)	3.47 (0.01)				2.84 (0.10)
140	0.89 (0.02)	0.11 (0.0)	2.37 (0.01)				1.94 (0.51)
160	0.90 (0.02)	0.10 (0.0)	1.54 (0.02)				1.26 (0.10)
180	0.91 (0.02)	0.09 (0.0)	1.50 (0.01)				1.23 (0.10)
200	0.93 (0.02)	0.07 (0.0)	1.39 (0.01)				1.14 (0.10)

Error at 68.2% of confidence interval (in brackets).

Figure 12 shows the variation of the hydraulic conductivity (moisture transfer coefficient) with the porosity of the tablet. The MTC decreases with the relative density in the same manner as the permeability. Because the water vapor was assumed to diffuse mostly through the interparticle pores of the tablet [29,46], the transfer of moisture from the tablet to the external environment depends on the tablet porosity. Hence, increasing the compression pressure led to the decrease of the overall porosity through which the water vapor diffuses. Therefore, water vapor migration might be slowed down because the path length of water vapor molecules becomes longer, due to the obstruction of the pores by the deformed powder particles. The abrupt decrease of the MTC in the low compactness region is due to the fast decrease of average porosity of the tablet and becomes steadier at a high compactness, where the average porosity is stabilized.

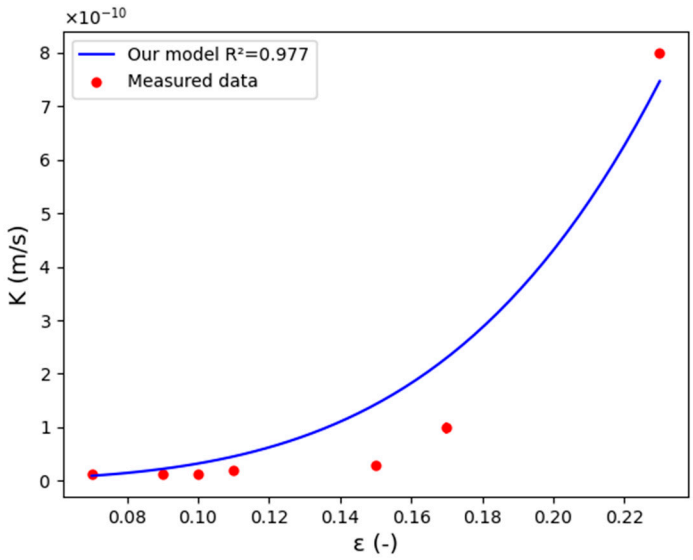

Figure 12. Variation of moisture transfer coefficient with the compressed MCC PH101 powder tablet porosity.

The model obtained for the permeability is used to predict the MTC values with a $R^2 = 0.977$. A similar model was found for hydraulic conductivity in porous media [29]. An exponential relation (Equation (23)), which can be implemented in the HAM model for simulation, is obtained between the normalized porosity and the normalized MTC with $R^2 = 1$ (Figure 13):

$$\frac{K}{K_0} = 2.55 \times 10^{-4} \exp\left(\frac{8.27 \times \varepsilon}{\varepsilon_0}\right) \quad (23)$$

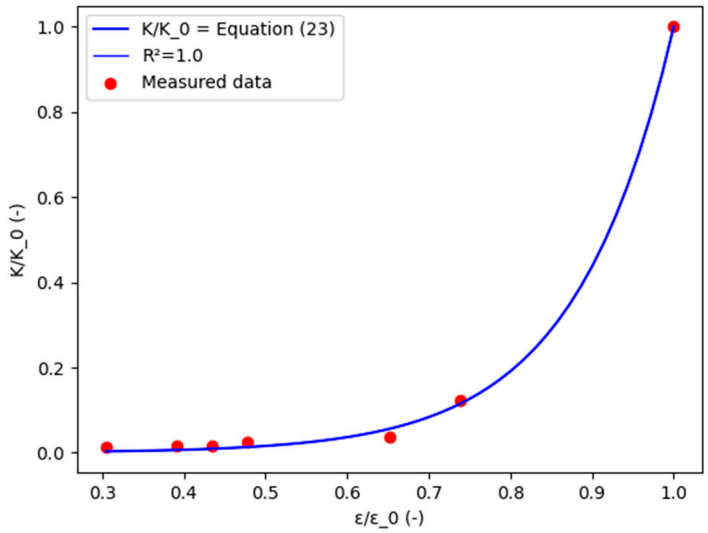

Figure 13. Variation of the normalized moisture transfer coefficient with the compressed MCC PH101 powder normalized tablet porosity.

3.4. Tablet Moisture Diffusion Coefficient

In this section, the moisture diffusion coefficient (MDC) in the compressed tablet was estimated. The MDC of the water vapor in the tablet during the compression depends on the flow regime [46]. The Knudsen number (Equation (9)) was estimated with the measured average pore radius to determine the diffusion regime followed by the water vapor in the tablet.

Table 5 lists the estimated value of the Knudsen number at each relative density using Equation (3).

Table 5. Calculated Knudsen number from the measured average tablet pores.

RD (-)	ε (-)	r ($\times 10^{-6}$ m)	P_B ($\times 10^5$ Pa)	R (J/(K·mol))	T (K)	M (kg/mol)	λ ($\times 10^{-7}$ m)	K_n (-)
0.69 (0.02)	0.31 (0.0)	2.83 (0.05)	1.01	8.314	293.15	0.018	5.92	0.21
0.74 (0.02)	0.26 (0.0)	1.25 (0.05)	1.02	8.314	293.15	0.018	5.92	0.47
0.77 (0.02)	0.23 (0.0)	1.03 (0.06)	1.03	8.314	293.15	0.018	5.92	0.58
0.79 (0.02)	0.21 (0.0)	0.76 (0.01)	1.04	8.314	293.15	0.018	5.92	0.84
0.83 (0.02)	0.17 (0.0)	0.75 (0.02)	1.05	8.314	293.15	0.018	5.92	0.78
0.84 (0.02)	0.16 (0.0)	0.68 (0.05)	1.06	8.314	293.15	0.018	5.92	1.02
0.89 (0.02)	0.11 (0.0)	0.76 (0.02)	1.07	8.314	293.15	0.018	5.92	0.78
0.90 (0.02)	0.10 (0.0)	0.69 (0.04)	1.08	8.314	293.15	0.018	5.92	0.70
0.91 (0.02)	0.09 (0.0)	0.72 (0.03)	1.09	8.314	293.15	0.018	5.92	0.82
0.93 (0.02)	0.07 (0.0)	0.74 (0.04)	1.10	8.314	293.15	0.018	5.92	0.63

Error at 68.2% of confidence interval (in brackets).

For each porosity value, the calculated Knudsen values range between $0.1 < Kn < 10$, which indicates that water vapor diffuses in the transitional flow regime, and the diffusion coefficient is the transitional one, D_{trans} (Equation (10)). Table 6 lists the calculated values of the transitional coefficient at different porosities.

Table 6. Calculated transitional diffusion at each relative density.

ε (-)	r ($\times 10^{-6}$ m)	R (J/(K·mol))	T (K)	M (kg/mol)	D_0 ($\times 10^{-5}$ m^2/s) [67]	D_k ($\times 10^{-4}$ m^2/s)	D_{trans} ($\times 10^{-5}$ m^2/s)
0.31 (0.0)	2.83 (0.05)	8.31	293.15	0.02	2.42	11.10	2.37 (0.0)
0.26 (0.0)	1.25 (0.05)					4.89	2.31 (0.0)
0.23 (0.0)	1.03 (0.06)					4.02	2.28 (0.01)
0.21 (0.0)	0.76 (0.01)					2.76	2.23 (0.0)
0.17 (0.0)	0.75 (0.02)					2.95	2.24 (0.0)
0.16 (0.0)	0.68 (0.05)					2.27	2.19 (0.0)
0.11 (0.0)	0.76 (0.02)					2.98	2.24 (0.0)
0.10 (0.0)	0.69 (0.04)					3.31	2.26 (0.01)
0.09 (0.0)	0.72 (0.03)					2.82	2.23 (0.01)
0.07 (0.0)	0.74 (0.04)					3.67	2.27 (0.0)

Error at 68.2% of confidence interval (in brackets).

The MDC of the water vapor decreases with the decrease of the porosity (Figure 14) due to the increase of the average bulk density of the tablet, until it stabilizes at the lower porosity.

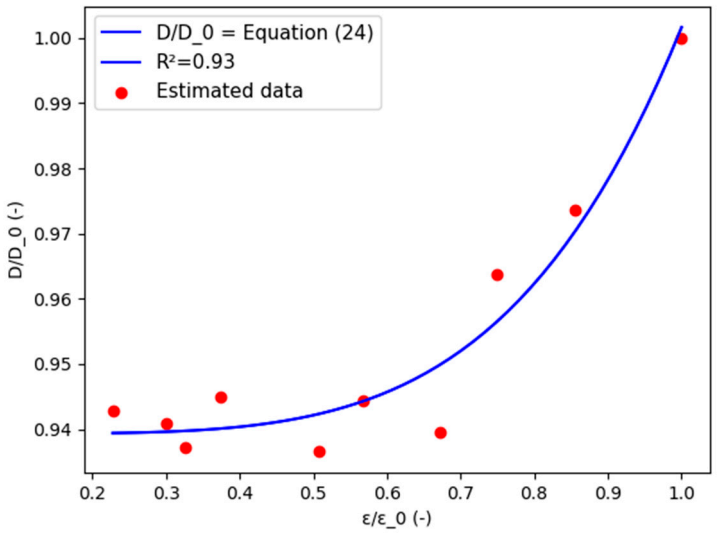

Figure 14. Variation of water vapor normalized diffusion coefficient with the compressed MCC PH101 powder tablet normalized porosity.

For simulation purposes, a power regression was used to fit the normalized MDC with the normalized average tablet porosity (Equation (24)). This equation can be implemented in the HAM model to simulate water vapor diffusion during the loading phase of the compression process and in the produced compressed powder tablet. The MDC was obtained from a tablet pore's radius-dependent formula (Equation (10)).

$$\frac{D}{D_0} = (6.28 \times 10^{-2}) \times \left(\frac{\varepsilon}{\varepsilon_0}\right)^{4.47} + 9.39 \times 10^{-1} \quad (24)$$

3.5. Water Vapor Permeability

Different semi-empirical and phenomenological models can be used to estimate the water vapor permeability (WVP), with the assumption that the vapor flow is laminar inside the porous material without any condensation: (1) the Woodside model [48] and the (2) Quenard and Sallée model (QS model) [52]. The full description of these models is presented in the Materials and Methods section. Because we considered the MCC tablet as a porous material with a certain range of porosity, these models can be used to estimate

the WVP. These models are valid and useful for unsaturated porous material with porosity ranging from 0 to 1; hence, they are applicable for MCC tablets. Moreover, we developed a semi-empirical model for the estimation of the WVP from the measured permeability and the estimation of the diffusion coefficient from the measured radius, as shown in Equation (25) (the values, predicted by the semi-empirical model developed in this study, were compared to those obtained with the Woodside and QS models in order to verify the usefulness of our method):

$$K_v = \frac{K_p}{D} \tag{25}$$

where *Kp* and *D*, respectively, are the permeability (m^2) and the water vapor diffusivity (m^2/s) in the tablet.

The WVP was estimated with the Woodside model, the QS model, and the model developed in this study (Table 7). The measured MDC and average pore radius was used for the QS model. Table 7 reports the estimated values of WVP with all models and Figure 15 depicts the results obtained with all models.

Table 7. Values of the water vapor permeability.

ε (-)	r ($\times 10^{-6}$ m)	Kp ($\times 10^{-16}$ m^2)	K_{air} ($\times 10^{-10}$ s)	D ($\times 10^{-5}$ m^2/s)	K_{vW} ($\times 10^{-10}$ s) (Woodside)	K_{vO} ($\times 10^{-10}$ s) (This Study)	K_{vQS} ($\times 10^{-7}$ s) QS Model
0.23 (0.0)	1.03 (0.06)	97.6 (0.6)		2.28 (0.01)	0.32 (0.0)	4.3 (1.50)	1.30 (0.05)
0.21 (0.0)	0.76 (0.01)	12.3 (0.1)		2.23 (0.0)	0.29 (0.0)	0.55 (1.80)	1.17 (0.04)
0.17 (0.0)	0.75 (0.02)	12 (0.1)		2.24 (0.0)	0.24 (0.0)	0.54 (0.01)	1.18 (0.03)
0.11 (0.0)	0.76 (0.02)	2.37 (0.01)	1.92	2.24 (0.0)	0.15 (0.0)	0.11 (0.0)	1. 18 (0.03)
0.10 (0.0)	0.69 (0.04)	1.54 (0.02)		2.22 (0.01)	1.32 (0.0)	0.07 (0.03)	1.13 (0.03)
0.09 (0.0)	0.72 (0.03)	1.50 (0.01)		2.23 (0.01)	1.19 (0.0)	0.07 (0.02)	1.15 (0.01)
0.07 (0.0)	0.74 (0.04)	1.39 (0.01)		2.27 (0.00)	0.09 (0.0)	0.06 (0.0)	1.17 (0.01)

Error at 68.2% of confidence interval (in brackets).

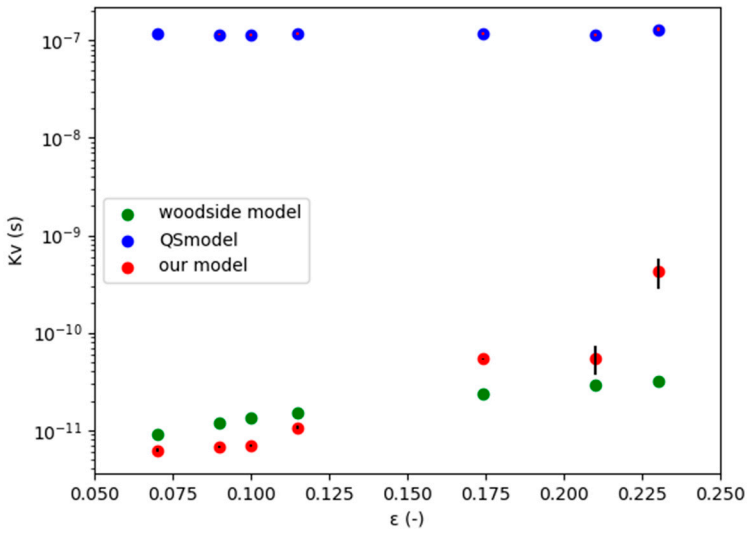

Figure 15. Water vapor permeability obtained with Woodside, QS, and our model.

The QS model gives values higher than free water vapor permeability in air (1.92×10^{-10} s) [48]. Because the diffusion flow regime of the water vapor in the compressed MCC tablet is found to be in the transitional regime, the WVP value can be assumed lower or in the same range with that of free water vapor in air. Hence, the QS model is considered to overestimate the WVP value. On the other hand, the Woodside model and our estimation fit well with that postulation. Due to the lack of experimental values in the literature, these later models are adopted in this study. Our calculus overestimated the

vapor permeability value at high porosity ($\varepsilon > 0.22$), which can be due to the pore network in the tablet.

An exponential regression (Equation (26)), for simulation purposes, was found between the normalized WVP and the normalized tablet porosity, with a regression coefficient $R^2 = 0.98$ (Figure 16):

$$\frac{K_v}{K_{v0}} = 2.10 \times 10^{-10} \exp\left(\frac{22.28 \times \varepsilon}{\varepsilon_0}\right) \quad (26)$$

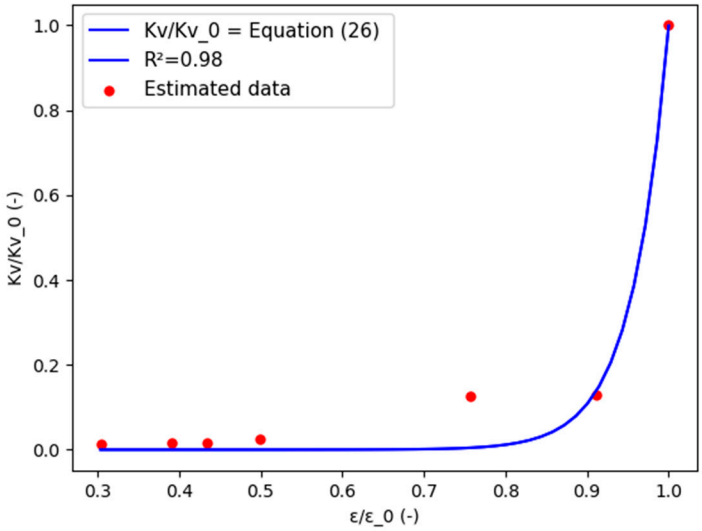

Figure 16. Variation of water vapor normalized permeability with the average compressed MCC PH101 powder tablet normalized porosity.

4. Conclusions

Several methods were presented in this study to determine moisture transport coefficients in MCC PH101 tablets. The ASTM D6539 standard test was used to measure the absolute permeability (AP), and a Carman-like model was proposed to predict the permeability in the tablet. This model is based on the tablets' microstructural parameters, which are porosity and pore radius. The average pores' radii was estimated with the water droplet penetration method, and the porosity was estimated with the tablet dimensions of the MCC tablets. However, the stability of the pores' average size, due to particle swelling with time, has to be further investigated. The moisture transfer coefficient (MTC) in the tablet was determined from the AP, with the passing gas characteristics and its value range classifying the MCC tablet as a semi-impervious material. Moisture was found to diffuse in the transitional regime, and the moisture diffusion coefficient (MDC) was estimated with the measured average pore radius. The water vapor permeability (WVP) obtained from the estimated MDC and the AP agreed with the Woodside model. The average porosity was found to control the behavior of the obtained moisture coefficients; therefore, a series of mathematical fits, using the porosity as a parameter, was proposed for simulation purposes.

These methods presented in this study can be used to estimate input parameters to simulate:

(1) the powder's moisture behavior during the loading phase of the compression to investigate problems such as delamination, caking, or sticking;
(2) the adsorption of moisture by the tablet after the ejection, which is known to weaken the tablet. However, since the pores' size can change with time due to particle swelling, a time-dependent factor must be eventually considered in the mathematical model.

In our next study, the input parameters obtained in this paper will be used to infer the sticking phenomenon through the powder moisture variation during the loading phase of the compression.

Supplementary Materials: The following supporting information can be downloaded at: https://www.mdpi.com/article/10.3390/pr10020254/s1, Table S1: Measured outflow (Q) and the calculated average outflow (Q_{av}); Table S2: Calculated Darcy permeability for each compressed powder tablet relative density.

Author Contributions: All the authors were involved in the conceptualization, methodology, the validation, and the formal analysis. Original draft preparation, K.K. All the authors were involved in review and editing, and visualization. Supervision, N.A. and F.G. All authors have read and agreed to the published version of the manuscript.

Funding: This work was funded by the Pfizer Chair on Process Analytical Technologies in Pharmaceutical Engineering.

Institutional Review Board Statement: Not applicable.

Informed Consent Statement: Not applicable.

Data Availability Statement: Not applicable.

Acknowledgments: This work was funded by the CRSNG Natural Sciences and Engineering Research Council. Thanks to the PRAM technicians of Université de Sherbrooke for their assistance with the powder properties measurements.

Conflicts of Interest: The authors declare no conflict of interest.

References

1. Gerad, K.; Bolhuis, N.; Armstrong, A. Excipients for direct compaction—An update. Pharmaceutical development and technology. *Pharm. Dev. Technol.* **2006**, *11*, 111–124. [CrossRef]
2. Sun, C.C. True density of microcrystalline cellulose. *J. Pharm. Sci.* **2005**, *94*, 2132–2134. [CrossRef] [PubMed]
3. Alderborn, G.; Ahlneck, C. Moisture adsorption and tabletting. III. Effect on tablet strength−post compaction storage time profiles. *Int. J. Pharm.* **1991**, *73*, 249–258. [CrossRef]
4. Malamataris, S.; Goidas, P.; Dimitriou, P.G. Moisture sorption and tensile strength of some tableted direct compression excipients. *Int. J. Pharm.* **1991**, *68*, 51–60. [CrossRef]
5. SunC, C. Mechanism of moisture induced variations in true density and compaction properties of microcrystalline cellulose. *Int. J. Pharm.* **2008**, *346*, 93–101. [CrossRef]
6. Newman, A.W.; Reutzel-Edens, S.M.; Zografi, G. Characterization of the "hygroscopic" properties of active pharmaceutical ingredients. *J. Pharm. Sci.* **2008**, *97*, 1047–1059. [CrossRef]
7. Crouter, A.; Briens, L. The Effect of Moisture on the Flowability of Pharmaceutical Excipients. *AAPS PharmSciTech* **2014**, *15*, 65–74. [CrossRef]
8. Zografi, G.; Kontny, M.J.; Yang, A.Y.S.; Brenner, G.S. Surface area and water vapor sorption of microcrystalline cellulose. *Int. J. Pharm.* **1984**, *18*, 99–116. [CrossRef]
9. Partheniadis, I.; Kopanelou, D.; Gamlen, M.; Nikolakakis, I. Monitoring the weight and dimensional expansion of pyridostigmine bromide tablets under dynamic vapor sorption and impact of deliquescence on tablet strength and drug release. *Int. J. Pharm.* **2021**, *609*, 121150. [CrossRef]
10. Shi, L.; Feng, Y.; Sun, C.C. Initial moisture content in raw material can profoundly influence high shear wet granulation process. *Int. J. Pharm.* **2011**, *416*, 43–48. [CrossRef]
11. Khan, F.; Pilpel, N.; Ingram, S. The effect of moisture on the density, compaction, and tensile strength of microcrystalline cellulose. *Powder Technol.* **1988**, *54*, 161–164. [CrossRef]
12. Amidon, G.E.; Houghton, M.E. The effect of moisture on the mechanical and powder flow properties of microcrystalline cellulose. *Pharm. Res.* **1995**, *12*, 923–929. [CrossRef] [PubMed]
13. Garr, J.S.M.; Rubinstein, M.H. The influence of moisture content on the consolidation and compaction properties of paracetamol. *Int. J. Pharm.* **1992**, *81*, 187–192. [CrossRef]
14. Choudhary, A. Causes and Remedies of Lamination in Tablet Manufacturing, Lamination in Tablets During the Compression is a Major Problem in Tablet Manufacturing. Available online: https://www.pharmaguideline.com/2017/11/causes-and-remedies-of-lamination.html (accessed on 30 October 2021).
15. Danjo, K.; Kojima, S.; Chen, C.Y.; Sunada, H.; Otsuka, A. Effect of water content on sticking during compression. *Chem. Pharm. Bull.* **1997**, *45*, 706–709. [CrossRef]
16. Takasaki, H.; Yonemochi, E.; Ito, M.; Wada, K.; Terada, K. The importance of binder moisture content in Metformin HCL high-dose formulations prepared by moist aqueous granulation (MAG). *Results Pharma Sci.* **2015**, *5*, 1–7. [CrossRef] [PubMed]
17. Blanchard, R. How Tablet Formulation Can Impact Production. 3 September 2019. Available online: https://www.europeanpharmaceuticalreview.com/article/98042/how-tablet-formulation-can-impact-production (accessed on 30 October 2021).

18. Leuenberger, H.; Rohera, B.D. Fundamentals of Powder Compression. I. The Compactibility and Compressibility of Pharmaceutical Powders. *Pharm. Res.* **1986**, *3*, 12–22. [CrossRef]
19. DeCrosta, M.T.; Schwartz, J.B.; Wigent, R.J.; Marshall, K. Thermodynamic analysis of compact formation; compaction, unloading, and ejection I. Design and development of a compaction calorimeter and mechanical and thermal energy determinations of powder compaction. *Int. J. Pharm.* **2000**, *198*, 113–134. [CrossRef]
20. Ketocaines, J.; Ilkka, J.; Parone, P. Temperature changes during tabletting measured using infrared thermoviewer. *Int. J. Pharm.* **1993**, *92*, 157–166. [CrossRef]
21. Wurster, D.E.; Buckner, I.S. Characterizing compaction-induced thermodynamic changes in a common pharmaceutical excipient. *J. Pharm. Sci.* **2012**, *101*, 2960–2967. [CrossRef]
22. Rowlings, C.E.; Wurster, D.E.; Ramsey, P.J. Calorimetric analysis of powder compression: II: The relationship between energy terms measured with a compression calorimeter and tableting behavior. *Int. J. Pharm.* **1995**, *116*, 191–200. [CrossRef]
23. Krok, A.; Mirtic, A.; Reynolds, G.K.; Schiano, S.; Roberts, R.; Wu, C.-Y. An experimental investigation of temperature rises during compaction of pharmaceutical powders. *Int. J. Pharm.* **2016**, *513*, 97–108. [CrossRef] [PubMed]
24. Zavaliangos, A.; Galen, S.; Cunningham, J.; Winstead, D. Temperature evolution during compaction of pharmaceutical powders. *J. Pharm. Sci.* **2008**, *97*, 3291–3304. [CrossRef] [PubMed]
25. Pitt, K.; Sinka, C. Chapter 16. Tabletting. In *Handbook of Powder Technology*; Elsevier: Amsterdam, The Netherlands, 2007; Volume 11, pp. 735–778. [CrossRef]
26. Klinzing, G.R.; Troup, G.M. Modeling the air pressure increase within a powder bed during compression—A step toward Understanding tablet defects. *J. Pharm. Sci.* **2019**, *108*, 1991–2001. [CrossRef] [PubMed]
27. Wünsch, I.; Finke, J.H.; John, E.; Juhnke, M.; Kwade, A. A mathematical approach to consider solid compressibility in the compression of pharmaceutical powders. *Pharmaceutics* **2019**, *11*, 121. [CrossRef]
28. Carman, P.G. Fluid flow through granular beds. *Trans. Inst. Chem. Eng.* **1937**, *15*, 150–166. [CrossRef]
29. Dos Santos, G.H.; Mendes, N. Combined Heat, Air and Moisture (HAM) Transfer Model for Porous Building Materials. *J. Build. Phys.* **2009**, *32*, 1744–2591. [CrossRef]
30. Bear, J. *Dynamics of Fluids in Porous Media*; Environmental science series; Elsevier: New York, NY, USA, 1972; ISBN 978-0-186-65675-5.
31. Pedersen, C.R. Prediction of moisture transfer in building constructions. *Build. Environ.* **1992**, *27*, 387–397. [CrossRef]
32. Luikov, A.V. *Heat and Mass Transfer in Capillary Porous Bodies*; Pergamon Press: Oxford, UK, 1966; ISBN 9781483225685.
33. Philip, J.R.; de Vries, D.A. Moisture movement in porous media under temperature gradients, trans. *Am. Geophys. Union* **1957**, *38*, 222–232. [CrossRef]
34. Hagentoft, C.E.; Kalagasidis, A.S.; Adl-Zarrabi, B.; Roles, S.; Carmeliet, J.; Hens, H.; Grunewald, J.; Funk, M.; Becker, R.; Shamir, D.; et al. Assessment method of numerical prediction models for combined heat, air and moisture transfer in building components: Benchmarks for one-dimensional cases. *J. Build. Phys.* **2004**, *27*, 327–352. [CrossRef]
35. Zavaliangos, A.; Katz, J.M.; Daurio, D.; Johnson, M.; Pirjanian, A.; Alvarez-Nunez, F. Prediction of air entrapment in tableting: An approximate solution. *J. Pharm. Sci.* **2017**, *106*, 3604–3612. [CrossRef]
36. El-Sabaawi, M.; Pei, D.C.T. Moisture isotherms of hygroscopic porous solids. *Ind. Eng. Chem. Fundam.* **1977**, *16*, 321–326. [CrossRef]
37. Kremer, D. A numerical investigation of air flow during tablet compression. *Chem. Eng. Sci.* **2006**, *61*, 7963–7978. [CrossRef]
38. COMSOL Multiphysics 5.4. Evaporation in Porous Media with Large Evaporation Rates. Available online: https://www.comsol.com/model/evaporation-in-porous-media-with-large-evaporation-rates-33731 (accessed on 30 October 2021).
39. Maliki, M.; Laredj, N.; Bendani, K.; Missoum, H.; Mostaganem, A.I.B.O. University Abdelhamid Ibn Badis of Mostaganem Two-Dimensional Transient Modeling of Energy and Mass Transfer in Porous Building Components using COMSOL Multiphysics. *J. Appl. Fluid Mech.* **2017**, *10*, 319–328. [CrossRef]
40. *ASTM D7481–18*; Standard Test Methods for Determining Loose and Tapped Bulk Densities of Powders using a Graduated Cylinder. Annual Book of ASTM Standards. ASTM: West Conshehoken, PA, USA, 2018. [CrossRef]
41. Rodríguez−Ramírez, J.; Méndez−Lagunas, L.; López−Ortiz, A.; Sandoval, T.S. True density and apparent density during the drying process for vegetables and fruits: A review. *J. Food Sci.* **2012**, *77*, 12. [CrossRef] [PubMed]
42. Hapgood, K.P.; Litster, J.D.; Biggs, S.R.; Howes, T. Drop penetration into porous powder beds. *J. Colloid Interface Sci.* **2002**, *253*, 353–366. [CrossRef] [PubMed]
43. Am Ende, D.J. *Chemical Engineering in the Pharmaceutical Industry: R&D to Manufacturing*; John Wiley & Sons: Hoboken, NJ, USA, 2011; ISBN 978-0-470-88222-1.
44. *ASTM E96/E96M−16*; Standard Test Methods for Water Vapor Transmission of Materials. Annual Book of ASTM Standards. ASTM: West Conshehoken, PA, USA, 2016. [CrossRef]
45. *ASTM D6539–13*; Standard Test Method for Measurement of the Permeability of Unsaturated Porous Materials by Flowing Air. Annual Book of ASTM Standards. ASTM: West Conshehoken, PA, USA, 2013. [CrossRef]
46. Klinzing, G.R.; Zavaliangos, A. A simplified model of moisture transport in hydrophilic porous media with applications to pharmaceutical tablets. *J. Pharm. Sci.* **2016**, *105*, 2410–2418. [CrossRef]
47. Vincenti, W.G.; Kruger, C.H. *Introduction to Physical Gas Dynamics*; Krieger Publishing Company: Malabar, FL, USA, 1965; p. 414. ISBN 0-88275-309-6.

48. Woodside, W. Water vapor permeability of porous media. *Can. J. Phys.* **1959**, *37*, 413–416. [CrossRef]
49. Edenholm, H. *Moisture Movement and Moisture Distribution in the Walls of Buildings*; National Research Council of Canada: Ottawa, ON, Canada, 1952. [CrossRef]
50. Penman, H.L. Gas and vapour movements in the soil: I. The diffusion of vapours through porous solids. *J. Agric. Sci.* **1940**, *30*, 437–462. [CrossRef]
51. Yang, B.; Wei, C.; Yang, Y.; Wang, Q.; Li, S. Evaluation about wettability, water absorption or swelling of excipients through various methods and the correlation between these parameters and tablet disintegration. *Drug Dev. Ind. Pharm.* **2018**, *44*, 1417–1425. [CrossRef]
52. Quenard, D.; Sallee, H. Water Vapor Adsorption and Transfer in Microporous Building Materials. a Network Simulation. In Proceedings of the Buildings Simulation Conference, Nice, France, 20–22 August 1991; pp. 31–36. Available online: http://www.ibpsa.org/proceedings/BS1991/BS91_031_36.pdf (accessed on 30 October 2021).
53. Westermarck, S. Mercury porosimetry of microcrystalline cellulose tablets: Effect of scanning speed and moisture. *Eur. J. Pharm. Biopharm.* **2000**, *50*, 319–325. [CrossRef]
54. Denesuk, M.; Smith, G.L.; Zelinski, B.J.J.; Kreidl, N.J.; Uhlmann, D.R. Capillary penetration of liquid droplets into porous materials. *J. Colloid Interface Sci.* **1993**, *158*, 114–120. [CrossRef]
55. Marston, J.O.; Thoroddsen, S.T.; Ng, W.K.; Tan, R.B.H. Experimental study of liquid drop impact onto a powder surface. *Powder Technol.* **2010**, *203*, 223–236. [CrossRef]
56. Eichheimer, P.; Thielmann, M.; Fujita, W.; Golabek, G.J.; Nakamura, M.; Okumura, S.; Nakatani, T.; Kottwitz, M.O. Combined numerical and experimental study of microstructure and permeability in porous granular media. *Solid Earth* **2020**, *11*, 1079–1095. [CrossRef]
57. Peng, X.; Boming, Y. Developing a new form of permeability and Kozeny–Carman constant for homogeneous porous media by means of fractal geometry. *Adv. Water Resour.* **2008**, *31*, 74–81. [CrossRef]
58. Kaviany, M. *Principles of Heat Transfer in Porous Media*, 2nd ed.; Springer: New York, NY, USA, 1995. [CrossRef]
59. Traxler, R.N.; Baum, L.A.H. Permeability of compacted powders determination of average pore size. *Physics* **1936**, *7*, 9. [CrossRef]
60. Bayles, G.; Klinzing, G.; Chiang, S. Fractal mathematics applied to flow in porous systems. *Part. Part. Syst. Charact.* **1989**, *6*, 168–175. [CrossRef]
61. Pape, H.; Clauser, C.; Iffland, J. Variation of permeability with porosity in sandstone diagenesis interpreted with a fractal pore space model. *Pure Appl. Geophys.* **2000**, *157*, 603–619. [CrossRef]
62. Civan, F. Scale effect on porosity and permeability: Kinetics, model and correlation. *AIChE J.* **2001**, *47*, 271–287. [CrossRef]
63. Costa, A. Permeability-porosity relationship: A reexamination of the Kozeny-Carman equation based on a fractal pore-space geometry assumption. *Geophys. Res. Lett.* **2006**, *33*, L02318. [CrossRef]
64. Zhang, D.; Tian, Z.; Chen, Z.; Wu, D.; Zhou, G.; Zhang, S.; Wang, M. Compaction effects on permeability of spherical packing. *Eng. Comput.* **2020**, *37*, 3079–3096. [CrossRef]
65. Huber, M.; Harvey, A. *Viscosity of Gases, CRC Handbook of Chemistry and Physics*; CRC Press: Boca Raton, FL, USA, 2011.
66. Helium, Jefferson Lab, U.S. Department of Energy. Available online: https://pubchem.ncbi.nlm.nih.gov/element/Helium#section=Density&fullscreen=true (accessed on 30 October 2021).
67. Lide, D.R.; Kehiaian, H.V. *CRC Handbook of Thermophysical and Thermochemical Data*; CRC Press: Boca Raton, FL, USA, 1994. [CrossRef]